A balanced homodyne detector and local oscillator shaping for measuring optical Schrödinger cat states

T. Gerrits*[a], S. Glancy[a], S.W. Nam[a]
[a]National Institute of Standards and Technology, 325 Broadway, Boulder, CO, USA 80305

ABSTRACT

We present our implementation of an optical homodyne detector used to measure optical Schrödinger cat states. We show how we minimized the losses and mode-mismatches associated with homodyne detection, which become important when measuring non-classical states of light. We present a pulse-shaping scheme applied to the local oscillator to improve its temporal mode overlap with the non-classical state.

Keywords: homodyne detection, optical Schrödinger cat states, squeezed vacuum

1. HOMODYNE DETECTION

1.1 Background

Homodyne detection is an important tool for the study of optical quantum states. A homodyne detector directly measures the phase dependent quadrature of the quantum state's electric field. Therefore homodyne detection enables continuous variable quantum key distribution schemes with classical and non-classical states [1-4]. It also allows phase estimations at the Heisenberg limit [5, 6]. Very interesting properties of non-classical states of light can be observed by use of homodyne detection, *e.g.* negatively valued Wigner distributions [7-10]. However, the observation of such features requires low loss in the detection of the input state. Interaction with the environment, *i.e.,* optical losses, mode mismatches, *etc.* degrade the measurement of the non-classical state. In the limit of high loss, the non-classical state will become a classical coherent state with small amplitude. In this paper we report on the development of a homodyne detector used for the generation of optical Schrödinger cat states used in an earlier study [10]. We define optical Schrödinger cat states as the superposition of two coherent states with opposite phase. We can approximate these states by photon-subtraction from squeezed vacuum [11]. We will describe the principle of homodyne detection, our homodyne detector, and adaptations to our optical setup in order to be able to measure the non-classical input state with low loss.

Figure 1 shows the general homodyne detection scheme. A strong local oscillator (coherent laser beam) and a weak quantum state signal (input state) are superimposed on a 50/50 beam splitter. Each output port of this beam splitter is monitored by high quantum efficiency photodiodes (PD1 and PD2). The individual output signals are subtracted and the resulting difference signal is recorded. A relative phase (ϕ) between the input state and local oscillator (LO) can be introduced by changing the relative optical path lengths. This allows measurement of the input state's quadrature as a function of phase angle.

The expectation values $\langle \hat{n}_i \rangle$,*i.e.*, measured output voltage, at output ports i = 1 and 2 after propagating the input modes through the beam splitter are $\langle \hat{n}_1 \rangle = \frac{1}{2}\left[\hat{a}^\dagger - \alpha_{LO}^*\right]\left[\hat{a} - \alpha_{LO}\right]$ and $\langle \hat{n}_2 \rangle = \frac{1}{2}\left[\hat{a}^\dagger + \alpha_{LO}^*\right]\left[\hat{a} + \alpha_{LO}\right]$, respectively. Subtracting these output signals and use of the relation $\hat{q}_\phi = \frac{1}{\sqrt{2}}\left[\left(\hat{a}^\dagger + \hat{a}\right)\cos\phi + i\left(\hat{a}^\dagger - \hat{a}\right)\sin\phi\right]$ leads to [12]:

$$\langle \hat{n}_2 \rangle - \langle \hat{n}_1 \rangle = \sqrt{2}\,|\alpha_{LO}|\,\hat{q}_\phi\,, \tag{1}$$

where $\hat{a}^\dagger$ $(\hat{a})$ is the creation (annihilation) operator, α_{LO} is the LO amplitude and $\hat{q}_\phi$ is the phase-dependent quadrature of the input state's electric field. Equation 1 shows that homodyne detection directly measures the projection of the input

Advanced Photon Counting Techniques V, edited by Mark A. Itzler, Joe C. Campbell,
Proc. of SPIE Vol. 8033, 80330X · © 2011 SPIE · CCC code: 0277-786X/11/$18
doi: 10.1117/12.885486

state's quadrature onto the LO field. Also, the output signal depends linearly on the LO strength. However, to measure a quantum state with high fidelity, low loss is required.

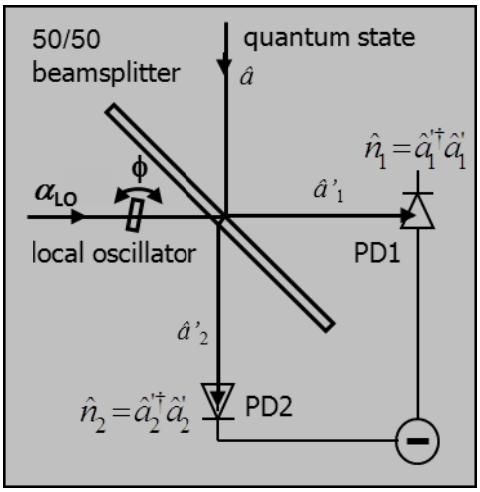

Figure 1. Homodyne detection schematic.

This imposes stringent requirements on all optical components used in the detection system, including the photodiodes. Also, because the homodyne detector measures the projection of the input mode onto the LO mode, the input mode should match the mode of the LO. Any mode-mismatch is equivalent to loss of the signal. Only when the input state is in a mode that matches the LO can perfect measurement fidelity of the input state be achieved. The mode matching must be achieved in the spatial, temporal and spectral domain. One can achieve better mode matching either by engineering the input state's output mode [13-16], or by tailoring the LO mode to match the input state output modes. In this paper we will present our efforts tailoring the LO in the spatial and temporal domain to match the input state's mode. Engineering of the input state to match the LO is described elsewhere [13].

1.2 Homodyne Detector

Figure 2 shows the electrical circuit layout for our homodyne detector. The homodyne detector is designed for charge integration and to operate at laser repetition rates of up to 1 MHz. Two fast Si PIN photodiodes are balanced to obtain the desired signal subtraction. The net signal is fed into a fast charge integrator designed to operate at ~1 MHz system repetition rate. We designed the circuit to suit a field effect transistor (FET) feedback resistor. This FET holds the charge until reset by an external voltage pulse. The last stage amplifies the output of the charge integrator by a factor of 10. The inset in figure 2 shows an example of responses from three similar Si PIN photodiodes. All three photodiodes were fabricated on the same substrate. One can see that the temporal responses are not perfectly identical. An identical temporal response is crucial for the homodyne circuit shown in figure 2. In case there is a slight difference in rise/decay times of the two photodiodes, subtraction of the signals will result in saturating the output amplification stage. Out of a set of six same-wafer photodiodes, we chose the two photodiodes that matched closest. We used a femtosecond laser pulse, centered at ~862 nm with a repetition rate of 548 kHz as the LO at the input of the 50/50 beam splitter in figure 1. Figure 3a shows ~6000 homodyne detector output traces, superimposed and plotted in the same graph. These data were taken without any input state in the second input port of the beam splitter. When the FET gate voltage is turned off, the charge integrator is ready to receive the net charge from the photodiodes. After the laser pulse hits the photodiodes, a dip in the output signal can be observed. This dip lasts several hundred nanoseconds and is due to the mismatch of the two photodiodes' temporal responses. We fine-tuned each of the bias voltages and scanned the laser spots across the active area of each of the two photodiodes to minimize the difference of the photodiodes' temporal response. After the photodiodes have released their charge, the homodyne output signal of interest can be observed. The FET switch then opens and releases the charge from the charge integrator.

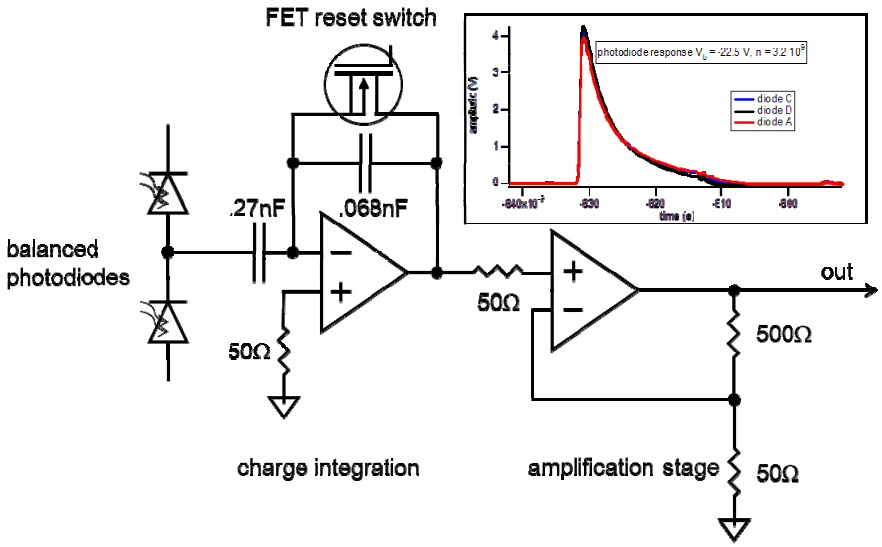

Figure 2. Homodyne detector circuit. The inset shows the individual responses from three same-wafer photodiodes.

When measuring our generated states we take eight data points within one repetition of the LO laser pulse (~4.4 MHz sampling rate). In order to minimize the shot noise induced by the FET, we chose one data point before and one data point after the laser pulse hits the photodiodes. Taking the difference of the two data points results in the homodyne detector output signal. We chose the two data points that resulted in the lowest electrical background noise. The electrical background noise is measured when blocking the LO and measuring the output signal alone. To calibrate the value of $|\alpha_{LO}|$ in (1), we measure the homodyne detector's output signal when only the vacuum is present in the input mode. The variance of this signal is proportional to the vacuum state's quadrature variance, which we set to 1, and the constant of proportionality is $2|\alpha_{LO}|^2$

The variance of the homodyne output scales linearly with the LO power, *i.e.,* photon number, owing to the shot noise of the coherent state input. Figure 3b shows the variance of our homodyne detector output as a function of input mean photon number. Clearly the output signal scales linearly with input photon number. The intercept with the ordinate is the electrical input noise level and is equivalent to 8250 electrons. The sensitivity of our homodyne detector is 230 nV/photoelectron, or 225 nV/photon, with photodiodes of ~98 % quantum efficiency at 862 nm.

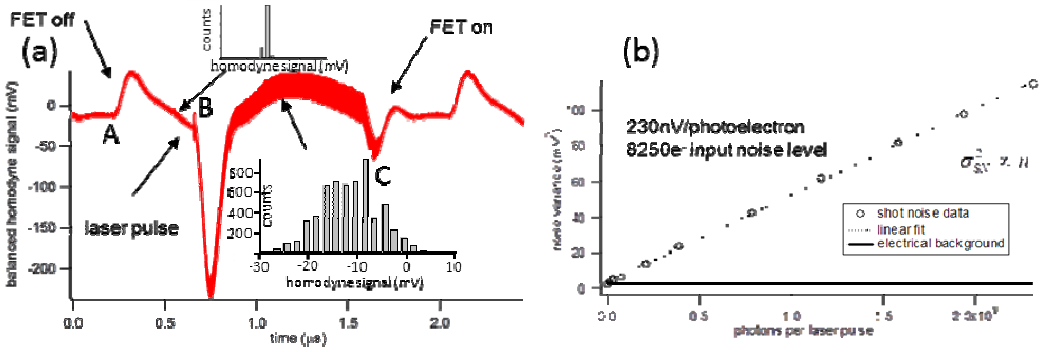

Figure 3. Homodyne detector output: (a) ~6000 consolidated homodyne traces: A: FET turned off, detector ready to receive net charge; B: laser pulse hits the photodiodes; C: FET turned on to reset the charge integrator. The insets show histograms of the homodyne detector output signal amplitude at (B) and (C), respectively (b) shot noise variance vs. input photon number

2. CAT STATE MEASUREMENT

2.1 Optical Schrödinger Cat State Generation Scheme

In the following we describe our cat state generation scheme and experimental setup as presented in ref. [10]. We can generate approximations to optical Schrödinger cat states when probabilistically subtracting photons from a pulse of squeezed vacuum [7-11]. Figure 4 shows the schematic of the cat state generation. A strong femtosecond laser pulse generates second-harmonics in a nonlinear crystal. This light then pumps a similar nonlinear crystal to generate the squeezed vacuum in a spontaneous parametric down-conversion process.

The squeezed vacuum is sent through a partially reflecting beam splitter where photons are probabilistically reflected (subtracted) from the squeezed vacuum. The subtracted photons are detected with a photon-number-resolving high-quantum-efficiency transition edge sensor [17]. When one or more photons are detected, a Schrödinger cat state approximation is generated, and a homodyne measurement is recorded.

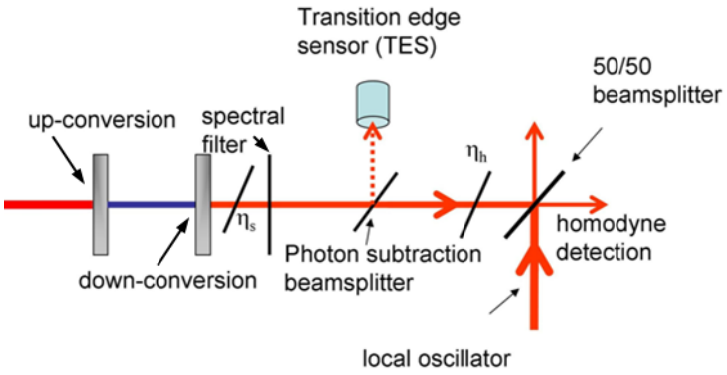

Figure 4. Schematic for optical Schrödinger cat state generation. Squeezed vacuum is generated in the down-conversion process. A partially reflecting beam splitter probabilistically subtracts and photons towards the TES. Upon detection of at least one photon, a Schrödinger cat state is generated and measured. η_h and η_s are the squeezing purity and total homodyne detection efficiency which can be modeled by a beam splitter with transmissivity η_h and η_s, respectively.

2.2 Squeezing

We model the squeezed vacuum generated in the experiment as a pure squeezed vacuum state with squeezed quadrature variance V_0, which has passed through a medium with transmissivity η_s. This state is then measured with the homodyne system whose efficiency is η_h; hence the measured efficiency is $\eta_m = \eta_h \eta_s$. (When measuring the squeezing directly, we set the reflectivity of the photon subtraction beam splitter to 0.) The observed squeezed V_p and anti-squeezed V_q variances are related to η_m and V_0 by [18]:

$$V_p = \eta_m V_0 + 1 - \eta_m,$$
$$V_q = \eta_m \frac{1}{V_0} + 1 - \eta_m. \tag{2}$$

Solving for η_m and V_0 gives

$$\eta_m = \frac{(1-V_q)(1-V_p)}{2-V_q-V_p},$$
$$V_0 = \frac{1-V_p}{V_q-1} \tag{3}$$

When we measured the squeezing matched to the LO using the pulse shaper described below, we observed V_q = 3.129 (+5.0 dB relative to vacuum variance) and V_p = 0.565 (-2.5 dB). After correcting for the overall homodyne detection efficiency η_h, we found η_s = 0.64 and an inferred squeezing variance of V_0 = 0.205 (-6.8 dB), based on equations 3. Pure squeezing is highly desirable for the generation of optical cat states. However, pure vacuum squeezing can be observed directly only when the LO matches the modes of the squeezed vacuum. In the remainder of this paper we describe how we adapted the LO to match the squeezed vacuum.

2.3 Experiment and Local Oscillator Shaping

Figure 5 shows the details of our experimental setup. We use a cavity-dumped femtosecond laser with transform-limited pulses of typically 140 fs duration and a repetition frequency of 548 kHz. The center wavelength of the cavity dumper output is λ_0 = 861.8 nm. Typical pulse energies are 40 nJ at the output port of the cavity dumper. We spatially filter the laser beam by sending it through a pinhole (PH) of 30 μm diameter. At the 90/10 beam splitter (BS) we split the laser beam into two parts. The weaker part of the beam is the strong LO (LO) for the homodyne detection (>10^9 photons/pulse). The stronger part pumps a 150 μm thick $KNbO_3$ crystal (SHG) to generate the second-harmonic pump photons. To eliminate any fundamental photons from the laser itself, we spectrally filter (SF) the second-harmonic pump. Then, the pump is focused into a 200 μm thick down-converting $KNbO_3$ crystal (OPA). Both crystals are temperature-tuned with stability better than 0.05 °C for optimum phasematching. Our optics in the homodyne detection arm after the down-converter eliminates most (>99.9 %) of the pump light, and its contribution to the homodyne signal is negligible. Therefore, no further spectral filtering is required after the OPA.

The squeezed vacuum is sent to the photon-subtraction beam-splitting components. The beam splitter consists of a half-wave-plate (HWP_1) and a polarizing beam splitter cube (PBS_1). The s-polarized waves experience less than 1% loss under reflection and the p-polarized waves undergo a 5 % loss due to transmission through the polarizing beam splitter. The reflected photons are sent to the homodyne detection arm, and hence the loss in this arm is minimized. The subtracted photons are directed to our spectral filter setup. It consists of a fiber Bragg grating (FBG) and a circulator. The FBG has a bandwidth of $\Delta\lambda_{FWMH}$ = 1.5 nm. The circulator is a combination of a free-space polarizing beam splitter (PBS_2) and quarter-wave-plate (QWP). This setup allows for good filtering of the subtracted photons. Upon detection of at least one photon at the photon number-resolving detector, we know that we have prepared an approximation of a cat state.

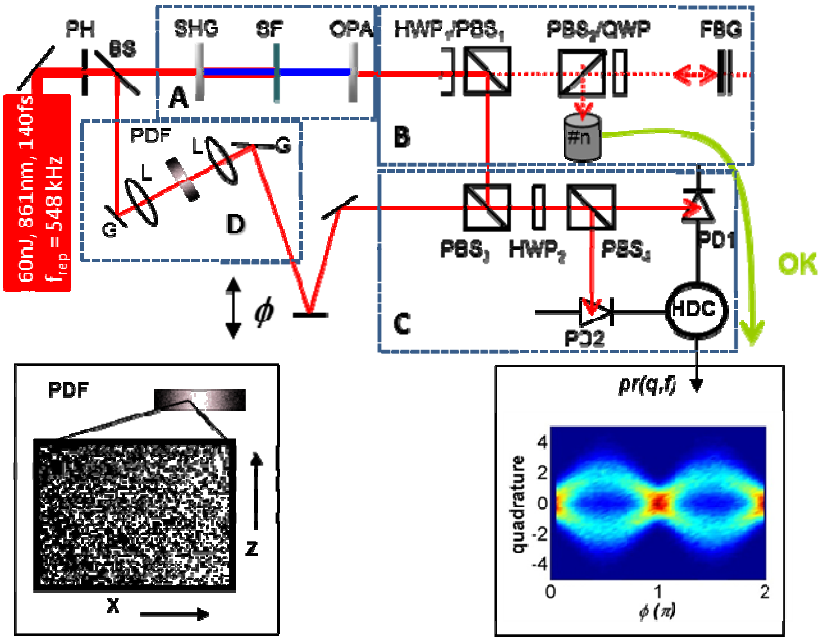

Figure 5. Detailed schematic of the experimental setup. Section A: up-conversion (SHG) to produce pump for the squeezed vacuum generation (OPA); Section B: photon subtraction to herald the presence of a cat state; Section C: homodyne detection; Section D: local oscillator temporal pulse shaping; left inset: sample pattern of the polka dot filter (PDF); right inset: quadrature data of a one-photon subtracted squeezed vacuum vs. phase angle

Homodyne measurements are recorded regardless of whether a photon is subtracted or not. When no photons are subtracted, a noisy squeezed state is measured, which we use to calibrate the phase of the LO. When a photon subtraction event occurs, the coincident homodyne measurement is tagged.

The phase of the LO is adjusted by a piezo-mounted mirror (ϕ). We continuously displace the mirror with a frequency of 2.75 Hz. The mirror's displacement is a saw-tooth profile with amplitude of about $2\lambda_0$. This allows a complete phase-space measurement of the input state. The LO and prepared cat state are combined at PBS_3. A half-wave-plate (HWP_2) and a polarizing beam splitter (PBS_4) constitute the 50/50 beam splitter necessary for the homodyne detection setup. Adjustment of HWP_2 allows for accurate balancing of the 50/50 ratio needed for the homodyne detection system. An intensity plot of a quadrature probability distribution after subtracting one photon from a squeezed vacuum is shown in the right inset of figure 5. The overall efficiency of the homodyne detection is $\eta_h = 0.853 \pm 0.028$. We have optimized this efficiency by the use of high-efficiency (> 97 %) photodiodes, low-loss (< 6 %) optical components, high spatial mode overlap (> 95 %) of the LO with the input state and low electrical background noise. The electrical background noise of the homodyne detectors and electronics is $e = V_e/(V_e + V_v) = 0.021 \pm 0.001$, where V_e is the variance of voltages measured when no light enters the photodiodes, and $V_e + V_v$ is the variance observed when only the LO is present ($V_e + V_v$ includes both electronic noise and shot noise of the LO). This is formally equivalent to an efficiency $\eta_e = (1\text{-}e) > 97.9$ % [19]. We also change the temperature of the up- and down-conversion crystals. The resulting changes in the phasematching conditions change the spectral output modes of the crystals and therefore change the squeezed vacuum output mode to match the LO. We scan both crystal temperatures in order to find the best temperature combination for the best squeezing. This method allows improving the squeezing purity by several percent. The temporal width of the LO is controlled by a pulse-shaping setup [20] so that we can compensate for the large mismatch in group velocity in our $KNbO_3$ crystals, which is ~1.2 ps/mm [21]. Using two gratings (G), two lenses (L) and a spatial filter, we can tune the temporal width of the LO from 140 fs to about 300 fs. The spatial filter is a polka dot filter (PDF) with Gaussian transmission profile to minimize possible chirp imposed by the pulse-shaping setup. We lithographically patterned these polka dot filters on chromium masks. In order to minimize and randomize the interference of the LO, which was sent through the PDF, we randomly distributed 4 μm × 4 μm squares along the z-axis of the filter. The squares' density changed according to a Gaussian envelope transmission profile along the x-axis of the filter. The filter design is shown in the left inset of figure 5. Different LO temporal widths are achieved by different PDF designs. The right inset of figure 5 shows the quadrature data of a one-photon subtracted squeezed vacuum as a function of phase angle acquired with our homodyne detection system.

Figure 6 shows the vacuum squeezing results as a function of LO temporal pulse width. Figure 6a shows the anti-squeezing (solid red line) and squeezing (solid blue line). A minimum in the squeezing value (highest down-conversion probability) can be observed at an LO pulse width of 190 fs. However, the highest down-conversion probability does not coincide with the highest squeezing purity, shown in figure 6b. For optical cat states we originally aimed for the highest squeezing purity possible, around 270 fs LO width. However, the highest fidelity cat state results were obtained for an LO width of 230 fs. When not using the PDF, we generally measured a squeezing variance $V_q = 2.15$ and $V_p = 0.67$, resulting in $\eta_s = 0.54$ after correcting for the homodyne detection efficiency. However, with the PDF in place, we achieved $V_q = 3.13$ and $V_p = 0.57$, resulting in $\eta_s = 0.64$.

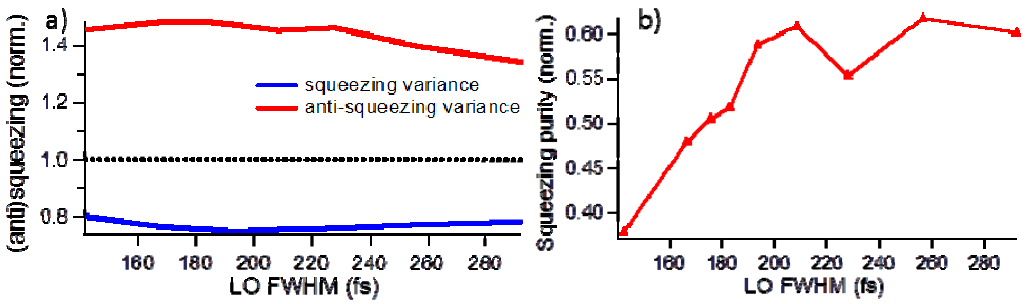

Figure 6. a) (anti)squeezing vs. LO pulse width; solid blue line: squeezing; solid red line: anti-squeezing b) squeezing purity vs. LO pulse width

3. SUMMARY

We presented our homodyne detection system and experimental setup for the generation and detection of optical Schrödinger cat states. We showed improvement in the squeezing purity of a squeezed vacuum when mode-matching the LO modes to the crystal output modes. Implementing an LO pulse shaping technique to match the temporal mode of the generated squeezed vacuum improved the squeezing purity significantly. We implemented a fast FET reset switch to allow for charge integrated balanced homodyne detection with a high signal to noise ratio and a repetition rate of up to 1 MHz.

4. REFERENCES

1. Reid, M.D., *Quantum cryptography with a predetermined key, using continuous-variable Einstein-Podolsky-Rosen correlations.* Physical Review A, 2000. **62**(6): p. 062308.
2. Ralph, T.C., *Security of continuous-variable quantum cryptography.* Physical Review A, 2000. **62**(6): p. 062306.
3. Hillery, M., *Quantum cryptography with squeezed states.* Physical Review A, 2000. **61**(2): p. 022309.
4. Grosshans, F., et al., *Quantum key distribution using gaussian-modulated coherent states.* Nature, 2003. **421**(6920): p. 238-241.
5. Dolinar, S.J., *An Optimum Receiver for the Binary Coherent State Quantum Channel.* MIT Research Laboratory of Electronics Quarterly Progress Report, 1973. **111**: p. 115-120.
6. Kennedy, R.S., *A Near-Optimum Receiver for the Binary Coherent State Quantum Channel.* MIT Research Laboratory of Electronics Quarterly Progress Report, 1973. **108**: p. 219-225.
7. Ourjoumtsev, A., et al., *Generating Optical Schrödinger Kittens for Quantum Information Processing.* Science, 2006. **312**(5770): p. 83-86.
8. Neergaard-Nielsen, J.S., et al., *Generation of a Superposition of Odd Photon Number States for Quantum Information Networks.* Physical Review Letters, 2006. **97**(8): p. 083604.
9. Wakui, K., et al., *Photon subtracted squeezed states generated with periodically poled KTiOPO4.* Opt. Express, 2007. **15**(6): p. 3568-3574.
10. Gerrits, T., et al., *Generation of optical coherent-state superpositions by number-resolved photon subtraction from the squeezed vacuum.* Physical Review A, 2010. **82**(3): p. 031802.
11. Glancy, S. and H.M. de Vasconcelos, *Methods for producing optical coherent state superpositions.* J. Opt. Soc. Am. B, 2008. **25**(5): p. 712-733.
12. Leonhardt, U., *Measuring The Quantum State Of Light* 1997: Cambridge University Press.
13. Gerrits, T., et al., *Characterization of high-purity, pulsed squeezed light at telecom wavelengths from pp-KTP for quantum information applications.* CLEO/QELS conference proceedings, Baltimore, MD 2011, 2011.
14. Grice, W.P., A.B. U'Ren, and I.A. Walmsley, *Eliminating frequency and space-time correlations in multiphoton states.* Physical Review A, 2001. **64**(6): p. 063815.
15. Mosley, P.J., et al., *Heralded Generation of Ultrafast Single Photons in Pure Quantum States.* Physical Review Letters, 2008. **100**(13): p. 133601.
16. Avenhaus, M., et al., *Fiber-assisted single-photon spectrograph.* Opt. Lett., 2009. **34**(18): p. 2873-2875.
17. Lita, A.E., A.J. Miller, and S.W. Nam, *Counting near-infrared single-photons with 95% efficiency.* Opt. Express, 2008. **16**(5): p. 3032-3040.
18. Bachor, H.A. and T.C. Ralph, *A Guide To Experiments In Quantum Optics*. 2004: Willey.
19. Appel, J., et al., *Electronic noise in optical homodyne tomography.* Physical Review A, 2007. **75**(3): p. 035802.
20. Weiner, A.M., *Femtosecond pulse shaping using spatial light modulators.* Review of Scientific Instruments, 2000. **71**(5): p. 1929-1960.
21. Weiner, A.M., A.M. Kan'an, and D.E. Leaird, *High-efficiency blue generation by frequency doubling of femtosecond pulses in a thick nonlinear crystal.* Opt. Lett., 1998. **23**(18): p. 1441-1443.